# Synthesis and characterization of carbon nanotubes decorated with Pt and PtRu nanoparticles and assessment of their electrocatalytic performance

Kardimi, Kiriaki; Tsoufis, Theodoros; Tomou, Aphrodite; Kooi, Bart J.; Prodromidis, Mamas I.; Gournis, Dimitrios

*Published in:*
International Journal of Hydrogen Energy

*DOI:*
10.1016/j.ijhydene.2011.09.143



*Publication date:*
2012

Available online at www.sciencedirect.com

SciVerse ScienceDirect

journal homepage: www.elsevier.com/locate/he

# Synthesis and characterization of carbon nanotubes decorated with Pt and PtRu nanoparticles and assessment of their electrocatalytic performance

*Kiriaki Kardimi* [a,b], *Theodoros Tsoufis* [a], *Aphrodite Tomou* [a], *Bart J. Kooi* [c], *Mamas I. Prodromidis* [b,**], *Dimitrios Gournis* [a,*]

[a] *Department of Materials Science & Engineering, University of Ioannina, GR-45110 Ioannina, Greece*
[b] *Department of Chemistry, University of Ioannina, GR-45110 Ioannina, Greece*
[c] *Zernike Institute for Advanced Materials, University of Groningen, Nijenborgh 4, NL-9747AG Groningen, The Netherlands*

ARTICLE INFO

*Article history:*
Received 14 July 2011
Received in revised form
28 September 2011
Accepted 30 September 2011
Available online 24 October 2011

*Keywords:*
Carbon nanotubes
Electrocatalyst
Nanoparticles
Pt
PtRu
Cyclic voltammetry

ABSTRACT

Novel hybrid electrocatalysts were developed based on the attachment of pre-formed capped Pt and PtRu nanoparticles (NPs) on the external surfaces of multi-walled carbon nanotubes (MWCNTs). MWCNTs chemically functionalized by both covalent and non-covalent chemical strategies were tested and evaluated as nanotemplates for the dispersion and stabilization of NPs. The suitable functionalized MWCNTs derivatives were then reacted with pre-formed capped Pt and PtRu NPs yielding the final hybrid materials. The intermediate products as well as the final hybrid materials were characterized in detail with a combination of experimental techniques including Raman spectroscopy, X-ray diffraction, scanning and transmission electron microscopy, while comparative studies regarding their electrocatalytic performance to the oxidation of methanol and ammonia, and to the reduction of hydrogen peroxide were made by performing cyclic voltammetry studies. The results revealed the uniform dispersion of very small NPs along the external surface of functionalized CNTs, while the most suitable electrocatalyst for each particular application is indicated. The chemical strategy followed for the surface functionalization of MWCNTs seems to greatly influence the catalytic activity of the resulting hybrids materials.



## 1. Introduction

Carbon nanotube (CNT) properties such as high specific surface area, thermal conductivity, and chemical stability, render them very attractive candidates for use as nanotemplates for the dispersion and stabilization of metal nanoparticles [1]. Metal nanoparticles (NPs) is a new class of materials exhibiting unique physical properties, clearly different from those of the bulk [2,3]. NPs have been proposed for many potential applications ranging from magnetism and biomedicine [4] up to cancer therapy [5] and catalysis [6]. Those properties are closely related to their size and shape [7–9]. Thus, of particular interest for NP science and technology are new synthetic strategies to control and,

* *Corresponding author*. Tel.: +30 26510 07141; fax: +30 26510 07074.
** *Corresponding author*. Tel.: +30 26510 08301; fax: +30 26510 08796.
E-mail addresses: mprodrom@cc.uoi.gr (M.I. Prodromidis), dgourni@cc.uoi.gr (D. Gournis).
0360-3199/$ – see front matter Copyright © 2011, Hydrogen Energy Publications, LLC. Published by Elsevier Ltd. All rights reserved.
doi:10.1016/j.ijhydene.2011.09.143

if possible, to adjust these NP's parameters [10,11]. By combining, the two classes of nano-materials (CNTs and NPs) novel hybrid materials can be synthesized that successfully incorporate the properties of the two counter-components. The formation of CNT-NP hybrids involves the absorption of NPs mainly to the CNT surface or alternatively, in the case of chemically functionalized NPs, their linkage to suitably functionalized CNTs through organic fragments. In general, there are two main pathways for the preparation of CNT–NP hybrids [12]. In the first strategy, pre-formed NPs can be linked to the CNT surface *via* covalent or weaker bonds. Therefore, the NPs are prepared and modified with suitable functional groups for the connection to the functionalized CNT surface. The linkers can be of two types: either functional groups, which may form covalent bonds with functional groups present on the CNT surface [13] or linkers that simply stick to the CNT surface through weak intermolecular interactions such as $\pi-\pi$ stacking [14] and/or electrostatic attractions [15,16]. An alternative pathway for the formation of CNT–NP hybrids, involves the direct reduction/deposition of the suitable NP precursor to CNT [17,18].

Pt is one of the most common catalysts in direct methanol fuel cells (DMFCs). However, Pt is easily poisoned by intermediate species such as CO, which are produced during methanol oxidation and thus suffers from the degradation of its catalytic activity [19]. To resolve such problem, Pt-based alloys such as PtRu, PtOs, and PtRuOs have been proposed, but since today the bimetallic Pt–Ru alloy has been considered to be the best candidate for the electrocatalysis of methanol oxidation reaction and is indeed the state of the art anode catalyst for DMFC [20,21]. The oxidation of adsorbed CO is postulated to be the rate-determining step and Ru is widely accepted as a promoter for the CO oxidation, commonly explained on the basis of the bifunctional mechanism or the ligand effect [22]. However, improvement of catalytic activity for the oxidation of methanol is an essential goal in the development of a practical DMFC with higher poison tolerance and greater methanol oxidation activity. CNTs as PtRu supports have generated intense interest in the fuel cell applications due to their unique properties and the reports that metal particles supported on the CNT seem to be less susceptible to CO poisoning than those deposited onto traditional carbon supports [23–25]. Since today, various methods have been proposed for the preparation of CNT–PtRu and CNT–Pt hybrids such as electrodeposition [26–30], nitrogen doping of CNT [31], microwaves [32,33], hydrothermal synthesis [34] and wet chemistry techniques [35–44].

Similarly to methanol, the electrocatalytic oxidation of ammonia in alkaline solutions is an important topic in the field of environmental chemistry [45], and sensors' development [46]. In addition, ammonia has attracted much attention as a possible fuel for fuel cells, since it is easy to handle and to transport compared with hydrogen gas [46,47]. The most widely accepted mechanism for ammonia oxidation was proposed by Gerischer and Mauerer since 1970 [48] and according to that, the ammonia molecule, after being adsorbed, is dehydrogenated to different adsorbed intermediate species of the type $NH_x$, where $0 \leq x \leq 2$. The final product of ammonia oxidation, nitrogen, is formed by reaction of these species with $OH^-$. While the partially dehydrogenated species of $NH_{2,ads}$ and $NH_{ads}$ are considered as active intermediates for $N_2$ formation, $N_{ads}$ remains strongly adsorbed on the surface acting as a poison [49]. A comparative study regarding the adsorption energy of $N_{ads}$ on various metals has shown that Pt is the best electrocatalyst [50], while the effect of other metals such as Ru, Pd, Rh, Ir, as Pt–Me binary systems on the electrochemical oxidation of ammonia has also been investigated [51].

Finally, the electrochemical reduction of $H_2O_2$ by employing metal-based catalysts has also attracted much attention, as $H_2O_2$, and more specifically, the enzymatically produced $H_2O_2$ is the basis for the development of a number of electrochemical biosensors based on oxidases [52]. In addition the electrochemical reduction of hydrogen peroxide is important in fuel cells as it is an intermediate product in oxygen reduction reaction especially in the acid media. A plethora of literature based on nano-sized materials such as CNTs [53], metal particles [39], porous Au [54] and highly roughened macroporous Au/Pt nanoparticles [55] have been widely investigated for their suitability as catalysts and chemical sensors. Moreover, the direct reduction of $H_2O_2$ has also been investigated at silver [56], gold [57], platinum [39], palladium [58] nanoparticles –modified electrodes, alone or in combination with CNTs [59].

In this work, we developed new chemical strategies for the attachment of pre-formed Pt and PtRu bimetallic NPs to chemically functionalized CNT and we evaluated the electrocatalytic properties of the resulting hybrid materials. The functionalization process debundles CNTs increasing their available surface area while introducing suitable available chemical groups (in high density) for the attachment of individual finely dispersed Pt and PtRu NPs. In detail, one of the employed strategies involved the covalent chemical functionalization of multi-walled carbon nanotube (MWCNT), yielding amino-terminated MWCNT derivatives. Since catalyst–support interactions play a fundamental role in catalysis, the surface functional groups responsible for anchoring the Pt and PtRu NPs to the CNT can greatly influence the catalytic activity of the resulting hybrids materials. An alternative synthetic approach was also used involving the non-covalent functionalization of MWCNT and the subsequent attachment of the Pt and PtRu NPs. The great advantage of this functionalization treatment is the conservation of MWCNT integrity and electronic structure, and therefore their electron conductivity. The synthesized hybrid materials were characterized by transmission and scanning electron microscopy, Raman spectroscopy and X-Ray diffraction measurements. In addition, the ability of these newly developed hybrid materials to serve as electrocatalysts, over a wide pH range, for compounds of great interest in fuel cells and (bio)chemical sensors technology was also studied. Comparative cyclic voltammetric studies of Pt and PtRu NPs supported on both covalently and non-covalently functionalized MWCNT–modified glassy carbon electrodes for the electrooxidation of methanol at pH <1, electroreduction of hydrogen peroxide at pH 7, and the electrooxidation of ammonia at pH >13 were performed and the most suitable electrocatalyst for each particular application is indicated.

## 2. Experimental

### 2.1. Chemicals

Platinum(II) acetylacetonate [$Pt(C_5H_7O_2)_2$], ruthenium(III) acetylacetonate [$Ru(C_5H_7O_2)_3$], diphenylether, 1, 2–dodecanediol, oleylamine, oleic acid, 1–pyrenemethylamine hydrochloride and multi-walled carbon nanotubes (length 0.5–500 μm, internal diameter 5–10 nm and external diameter 10–30 nm) were obtained from Aldrich. Thionyl chloride ($SOCl_2$), dimethylforamide (DMF) and 1, 6–hexamethylenediamine were purchased by Merck. Methanol, hydrogen peroxide (30% w/w) and aqueous ammonia (25% w/w) were purchased from Riedel-de Haen. Double distilled water (DDW) was used throughout. All other chemicals were of analytical grade from Merck and Sigma.

### 2.2. Synthesis of capped Pt nanoparticles

Monodispersed Pt capped NPs were prepared by the polyol synthetic procedure [60]. In detail, diphenylether (20 mL), 1, 2–dodecanediol (10 mmol) and oleylamine (5 mmol) were mixed in a spherical flask (50 mL) and refluxed under continuous stirring at 140 °C for 10 min. Platinum(II) acetylacetonate (1.5 mmoL) and oleic acid (5 mmoL) were added afterwards in the solution and the temperature was raised up to 180 °C. The reaction took place under these conditions for 3 h and the mixture was then cooled at RT (Fig. 1A). The Pt capped NPs were precipitated with absolute ethanol (40 mL) and isolated by centrifugation. The precipitates were washed several times with ethanol, centrifuged and the final (Pt capped NPs) precipitate was dispersed with acetone and then dried at RT.

### 2.3. Synthesis of capped PtRu nanoparticles

Monodispersed PtRu capped NPs were prepared in a similar way as Pt capped $NP_S$ by adding equimolar amounts (1.5 mmoL) of each metal precursor.

### 2.4. Chemical functionalization of carbon nanotubes

MWCNTs were chemically functionalized according to previously reported chemical routes for covalent [13,61] and non-covalent functionalization [62]. In brief, for the covalent functionalization of MWCNTs, pristine nanotubes (100 mg) were suspended in 80 mL of a concentrated $H_2SO_4/HNO_3$ mixture (3 : 1) and sonicated for 3 h for the generation of oxygen-containing functional groups (Fig. 1B–i). The suspension was then centrifuged and washed six times with DDW and dried at 50 °C in vacuum overnight. The carboxylated MWCNTs were suspended in a mixture of 50 mL thionyl chloride and 2 mL DMF and were further refluxed (Fig. 1B-ii). The acyl–clorinated MWCNT derivatives were centrifuged, washed with anhydrous toluene, and dried under high vacuum. The dry product (~95 mg) was then dispersed in 95 mL $CHCl_3$ and reacted with an excess quantity of 1, 6–hexamethylenediamine (191 mg) diluted in 96 mL $CHCl_3$ to yield the poly-amine terminated MWCNT derivatives (Fig. 1B-

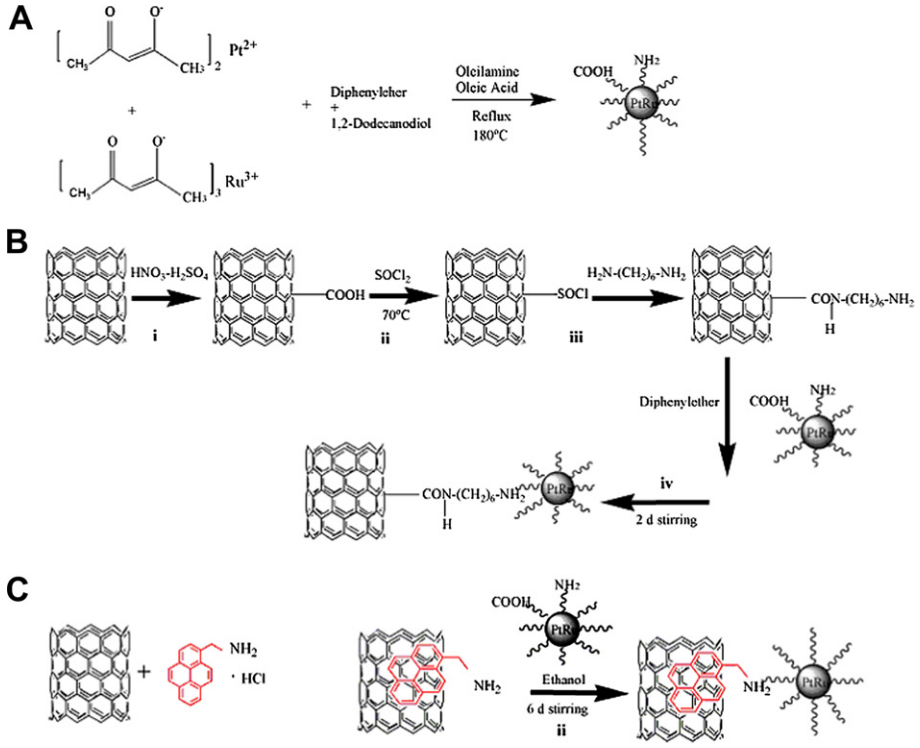


**Fig. 1 – Schematic representation of the procedures followed for the A) synthesis of capped PtRu NPs by the polyol process, B) chemical functionalization of MWCNTs and covalent linking of capped NPs and C) non-covalent functionalization of MWCNTs followed by subsequent attachment of NPs.**

iii). The final material was dried in vacuum at room temperature and collected as black powder. For the non-covalent functionalization of the MWCNT, a certain quantity of pristine CNTs (20 mg) was sonicated in an ethanol solution containing 1–pyrenemethylamine hydrochloride (20 mg) for 2 h under nitrogen atmosphere (Fig. 1C–i). Then, the mixture was stirred overnight and the final amino derivatives of the MWCNT were isolated from the solution by centrifugation and washed with ethanol.

### 2.5. Preparation of MWCNT–Pt and MWCNT–PtRu hybrids

Covalently functionalized CNT (*CF*–CNT) and non-covalently functionalized CNT (*NCF*–CNT) were further functionalized with each of Pt– and PtRu– capped NPs thus occurring four novel hybrid materials: *CF*–CNT/Pt, *CF*–CNT/PtRu, *NCF*–CNT/Pt and *NCF*–CNT/PtRu. In brief, a certain amount of Pt and PtRu capped NPs was dissolved in diphenylether and added to a dispersion of *CF*–CNT and *NCF*–CNT in diphenylether so as the weight ratio of NPs to MWCNTs to be 10 (*CF*–CNT/Pt), 5 (*CF*–CNT/PtRu) and 3 (*NCF*–CNT/Pt and *NCF*–CNT/PtRu). The mixture was sonicated and left under stirring for several days. The synthesized hybrids for each occasion (Fig. 1B-iv and C-ii) were separated by centrifugation, washed several times with pure ethanol and dried under vacuum at room temperature.

### 2.6. Characterization studies

Transmission electron micrographs were obtained using a JEOL JEM-2010F microscope (operating at 200 kV) equipped with an EDAX detector. For the preparation of TEM samples a drop of the corresponding solution in hexane was deposited onto a holey-carbon grid and left to evaporate. Scanning electron images were recorded using a JEOL JSM-5600V scanning electron microscope. All images are typical and representative of the samples under observation. Raman spectra were recorded with a Micro-Raman system RM 1000 RENISHAW using a laser excitation line at 532 nm (Nd-YAG) in the range of 1000–2400 $cm^{-1}$. A 0.5–1 mW laser was used with 1 μm focus spot in order to avoid photodecomposition of the samples. X–ray powder diffraction data were collected on a D8 Advance Bruker diffractometer using Cu–$K_\alpha$ radiation and a secondary beam graphite monochromator. The patterns were recorded in the 2–theta (2θ) range from 20° to 90°, with steps of 0.02° and a counting time of 2 s per step.

### 2.7. Electrochemical studies

All electrochemical measurements were conducted with the electrochemical analyzer PGSTAT12 (Metrohm Autolab) at room temperature. Cyclic voltammetric experiments were performed in a 3-electrode cell. Modified or bare glassy carbon (GC) electrodes (3 mm diameter, IJ Cambria) and a platinum wire were served as the working and auxiliary electrodes, respectively. The reference electrode was a Ag/AgCl/3 M KCl (IJ Cambria) electrode and all potentials reported hereafter refer to the potential of this electrode. The flow injection experiments were carried out, by using an in-house fully automated flow injection manifold. The carrier stream (0.2 M phosphate buffer, pH 7 in 1 M KCl) was pumped through using a 4-channel peristaltic pump (Gilson) and standard solutions of $H_2O_2$ were introduced as short pulses of 130 μL *via* a pneumatically actuated injection valve (Rheodyne). The working electrode (bare or Pt NPs or *CF*–CNT/Pt –modified GC electrodes) was mounted in a 3-electrode wall-jet cell (volume <1 μl) consisting of a built-in gold auxiliary electrode and a Ag/AgCl/3 M KCl reference electrode.

### 2.8. Preparation of the modified electrodes

Suspensions of 0.5 mg $mL^{-1}$ PtRu NPs, *CF*–CNT/Pt or *CF*–CNT/PtRu and 1.0 mg $mL^{-1}$ *NCF*–CNT/Pt or *NCF*–CNT/PtRu, were prepared by mixing the appropriate amount of the catalysts in THF. After sonication for 10 min, suspensions were vigorously stirred for 48 h before use. Prior to the modification, GC electrodes were polished with aluminum oxide (0.01 μm), rinsed thoroughly with DDW, sonicated for 1 min in DDW, rinsed with DDW and dried under Ar. Modification of the GC electrodes was achieved by dropping 10 μL of PtRu NPs, *CF*–CNT/Pt, *CF*–CNT/PtRu, *NCF*–CNT/Pt or *NCF*–CNT/PtRu suspensions over the active surface and left the solvent to evaporate overnight.

## 3. Results and discussion

### 3.1. Characterization studies

Transmission electron microscopy (TEM) images show the successful attachment of PtRu nanoparticles to the surface of the chemically functionalized carbon nanotubes and in addition provide information about their size and state of dispersion. In detail, lower magnification TEM images of *CF*–CNT/PtRu hybrids (Fig. 2A–B) reveal the homogeneous dispersion of uniform sized PtRu NPs along the covalently functionalized MWCNT with relatively high particle density and without the formation of any noticeable aggregates. Higher resolution TEM images (Fig. 2C), further confirmed the successful decoration of nanotubes with PtRu NPs. Based on several different TEM images, the average size of the highly dispersed PtRu NPs was estimated about 2.5 nm. The characteristic (111) and (200) planes, as will be shown below likely originating from the face-centered cubic (fcc) crystal structure of the platinum phase, were also resolved (Fig. 2C). Moreover, the presence of hollow MWCNTs (of about 35 nm outer diameter) among the final hybrid materials, suggests that the nanotubes remain relative intact after oxidation and chemical functionalization, surviving the acid treatment without showing any significant damage to their tubular graphitic structure. A more representative image of the nanotubes after acid treatment and 1, 6–hexamethylenediamine functionalization steps is given with the low magnification SEM image in Fig. 2D. Similar images were taken for the non-covalently functionalized CNT (Fig. 2E) as well.

The reflections originating from the *CF*-CNT/Pt and *CF*-CNT/PtRu hybrids were also recorded in X-Ray diffraction patterns (Fig. 3A). In detail, the main diffraction peaks of the *CF*–CNT/Pt hybrid (Fig. 3Aii) at $2\theta \approx 39.5°$, 46.3° and 67.4° can be assigned respectively to the (111), (200) and (220) crystalline

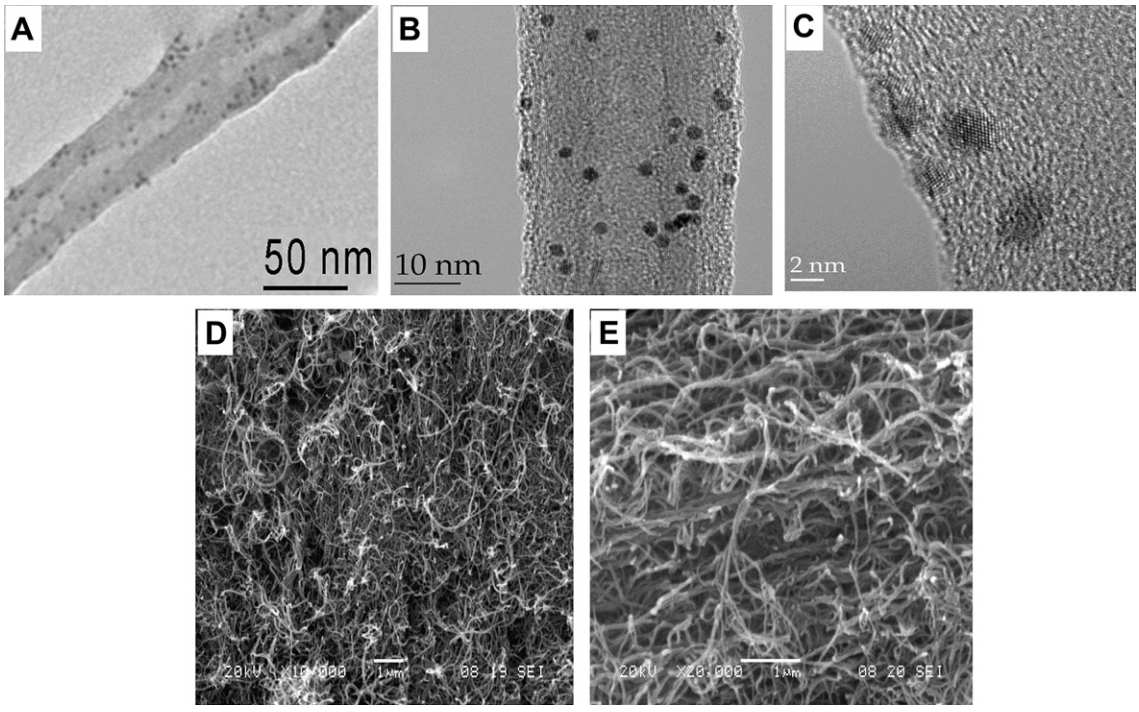


**Fig. 2 – (A–B) Low and (C) high magnification TEM images of *CF*–CNT/PtRu hybrids; SEM images of (D) 1, 6–hexamethylenediamine functionalized CNT and (E) *NCF*–CNT/PtRu.**

planes of the fcc platinum phase. Using the Scherrer equation, the mean crystallite size of the attached Pt particles was estimated about 3.1 nm, a value very similar to the corresponding value found for the free Pt NPs (Fig. 3Ai) used for the synthesis of the *CF*–CNT/Pt hybrids. Analogous diffraction peaks were recorded in the case of the *CF*–CNT/PtRu hybrid materials. The "absence" of diffraction peaks typical for Ru can be due to a number of reasons such as Ru being dissolved into the Pt lattice, i.e. a PtRu alloy is formed that maintains the fcc Pt structure. This is very likely, because the Pt–Ru phase diagram shows excellent solubility of Ru of more than 50% in Pt in the solid phase [63]. Another, less likely, reason can be that Ru is present in the amorphous form [64]. It is interesting to note that the "absence" of the Ru (101) plane (which represents the most intense reflection of the hexagonal Ru pattern) from the XRD patterns, is reported in several previously cases of successfully synthesized PtRu NPs [22,65,66]. Moreover, additional EDS measurements (not discussed here in detail) for both *NCF*– and *CF*–MWCNT/PtRu samples, revealed the presence of Ru in both types of final hybrid materials with the identical value of % atomically ratio (1:4 in particular) compared with Pt. Therefore, it is most likely that the NPs are composed of an PtRu alloy that has the same fcc structure as pure Pt.

In addition, a broadening of the reflection peaks followed by a decrement of their intensity was observed in the case of the *CF*–CNT/PtRu hybrids (Fig. 3Aiv) due to the smaller crystallite size of the synthesized PtRu NPs (Fig. 3Aiii) that were used for their synthesis. Indeed, using the Scherrer equation, the mean crystallite size of the PtRu particles was estimated about 2.3 nm, a value considerably lower than the corresponding value of the Pt NPs used for the synthesis of *CF*–CNT/Pt hybrids. Notably, the estimated crystallite size of the PtRu NPs is in agreement with corresponding particle size as emerged from the previously described TEM measurements (cf. Fig. 2). Similar findings were observed in the case of the hybrids synthesized using non-covalently functionalized CNT. As in the case of amino functionalized CNT, based on the XRD patterns of the final synthesized hybrids, Pt and PtRu particles with corresponding estimated sizes of 2.3 and 3 nm were found among the final hybrid materials. Moreover, the characteristic diffraction peak at $2\theta \approx 26^{\circ}$, originating from the 002 graphitic reflection of MWCNT (Fig. 3Bii and Biii), was clearly recorded in the patterns of both MWCNTs final hybrids. The appearance of this characteristic diffraction peak could be due to the lower functionalization degree that took place in the case of the 1–pyrenemethylamine resulting in lower debundling of the MWCNT network and thus at lower coverage of the functionalized MWCNT with Pt or PtRu NPs. This hypothesis is supported by the fact that non-covalent functionalization strategies result in the introduction of fewer chemical functional groups at the surface of CNT compared to covalent methods.

Raman measurements further confirmed the existence of MWCNT in the final hybrids and provided additional information regarding their electronic state. Among other peaks, the two peaks characteristic for MWCNT [67] were recorded in all Raman spectra of the various MWCNT derivatives and final hybrids. In detail, the G (graphite) band at 1595 $cm^{-1}$ corresponds to the Raman-active $E_{2g}$ mode of graphite due to $sp^2$-hybridized carbons, while the D (defect) band at 1314 $cm^{-1}$ is attributed to either $sp^3$-hybridized carbons or to structural

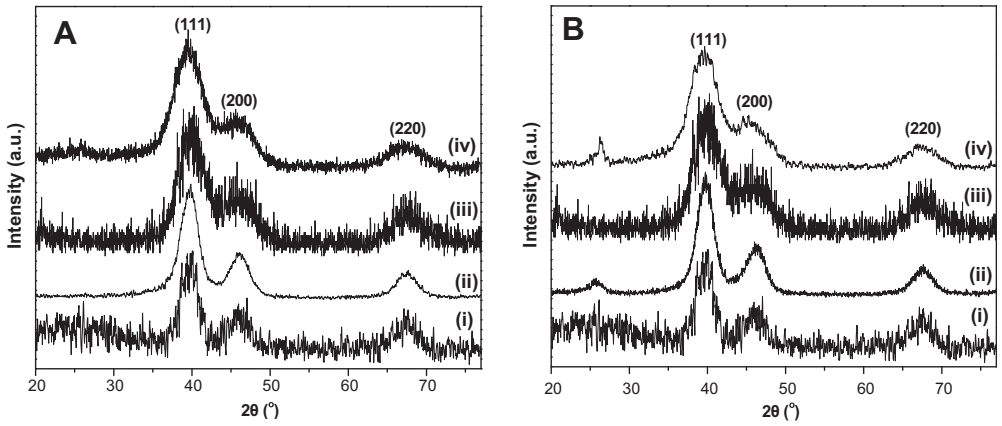


**Fig. 3 – XRD patterns of (A) free Pt NPs (i), *CF*–CNT/Pt hybrids (ii), free PtRu NPs (iii), *CF*–CNT/PtRu hybrids (iv), and (B) Pt NPs (i), *NCF*–CNT/Pt hybrids (ii), free PtRu NPs (iii) and *NCF*–CNT/PtRu hybrids (iv).**

defect sites of the $sp^2$-hybridized carbon network. In the Raman spectrum of the pristine MWCNT (Fig. 4Ai), the calculated value of the relative intensity ratio of the D to G band ($I_D/I_G$) was found relative high (0.96), indicating that the starting MWCNT already contain a high defect concentration and/or high non-CNT graphitic impurities. In the case of the covalently functionalized MWCNT (Fig. 4Aii), the spectrum is slightly different from the pristine nanotubes, exhibiting only a small, if any, decrement in the $I_D/I_G$ ratio in the case of the final MWCNT derivative (0.95). This behavior is not unusual for covalently functionalized MWCNT [68] since the functionalization does not bring any dramatic increment of the $sp^3$ carbons because it takes place solely on the outer graphene layer [69]. Similar results were found in the case of the non-covalently functionalized MWCNT derivative (Fig. 4Aiii). In their case, although a broading of mainly G-band was recorded, the corresponding value of the relative $I_D/I_G$ ratio (0.97) remained practically intact compared to the starting nanotubes due to the π-π interactions of the pyrenemethylamine with only the outer graphene layer of the nanotubes, resulting into a minor distortion of the nanotube electronic structure. The presence of both characteristic graphitic bands in the spectra of all final hybrids (Fig. 4B) without any additional striking changes in the value of their relative $I_D/I_G$ ratios, further confirm the presence of MWCNT among them without any additional, significant changes in their electronic structure compared to their corresponding functionalized derivatives. In detail, in the case of *CF*–CNT/PtRu and *CF*–CNT/Pt hybrids the value of the relative intensity ratios was found 0.97 and 0.96, respectively (Fig. 4Bi, Bii). In the case of the non-covalently functionalized nanotubes, the values of the *NCF*–CNT/PtRu and *NCF*–CNT/Pt hybrids were found 0.97 and 0.98, respectively (Fig. 4Biii, Biv).

### 3.2. *Assessment of the electrocatalytic performance*

The electrocatalytic performance of the newly synthesized hybrids materials was evaluated with cyclic voltammetry studies of properly modified glassy carbon (GC) electrodes using methanol, hydrogen peroxide and ammonia as tested analytes. In addition, the analytical utility of the best performing hybrid catalyst of the electroreduction of hydrogen peroxide was further tested with amperometric flow injection analysis measurements.

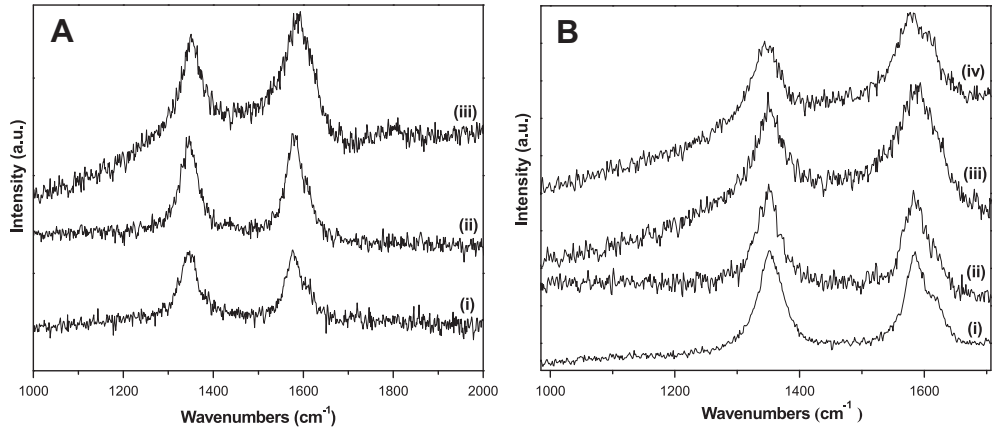


**Fig. 4 – Raman spectra of (A) pristine MWCNT (i), covalently functionalized MWCNT (ii) non-covalently functionalized MWCNT (iii) and (B) of *CF*–CNT/Pt (i), *CF*–CNT/PtRu (ii), *NCF*–CNT/Pt (iii) and *NCF*–CNT/PtRu (iv).**

At the offset, the proposed catalysts were dispersed in different media in order to conclude the optimum dispersing agent for the modification of the electrodes. The parameters that have been taken into account include i) the life-time of the suspension, ii) the surface tension of the suspension onto the surface of the electrode, iii) the evaporation rate of the solvent, iv) the storage stability of the modification suspension and v) the sensitivity of the resulting sensors. As a measure the height of the electrocatalytic current at 0.0 V in the presence of 20 mM $H_2O_2$ was taken and comparative experiments were performed with *CF*–CNT/PtRu catalyst in a concentration of 1 mg per mL solvent. As can be seen in Fig. 5, best results were obtained for THF and THF/formic acid mixtures. Due to the limited storage stability of THF/formic acid mixtures, THF was selected for further experiments.

### 3.2.1. *Electrocatalytic reduction of hydrogen peroxide*

The values of the catalytic current, $I_{cat}$, for the electroreduction of $H_2O_2$, corrected for the background signal ($I_b$, in the absence of $H_2O_2$), which are tabulated in Table 1 show that both PtRu NPs– and *CF*–CNT/PtRu–modified electrodes exhibit optimum performance at a concentration of 0.5 mg/mL of the modifier, and more interestingly, that the CNT supported catalysts provide an almost 50% higher catalytic activity, even though the amount (% atom) of the nanoparticles in *CF*–CNT/PtRu hybrid material is roughly 10%, according to the EDS data. According to similar optimization studies (data not shown), *CF*–CNT/Pt and both the *NCF*-based materials showed an optimum performance at a deposition concentration of 0.5 mg $mL^{-1}$ and 1.0 mg $mL^{-1}$, respectively.

At the optimum concentration for each material, a comparative CV study was obtained, as is illustrated in Fig. 6. The pattern of the CV-grams is indicative of the ability of all of the tested hybrid materials to catalyze the electroreduction of hydrogen peroxide, while in terms of sensitivity (maximum peak height at the potential range from −0.1 to 0.2 V), the tested catalysts can be classified as: *CF*–CNT/PtRu > *NCF*–CNT/PtRu > *CF*–CNT/Pt > *NCF*–CNT/Pt. An important conclusion of this classification is that the heterogeneous catalysts containing the bimetallic catalyst PtRu found to be the most effective, thus indicating the contribution of Ru to the electroreduction of hydrogen peroxide.

Another issue of great analytical importance is the working stability (reusability of the catalyst and adhesion of the hybrid material on the surface of the electrode) of the *CF*–CNT/PtRu modified GC electrodes. Working under flow conditions, the proposed sensors showed a remarkable stability for at least 45 successive injections of 0.1 μM $H_2O_2$. As can be seen in Fig. 7, PtRu NPs modified GC electrodes showed an excellent working stability as well, while the benefit from the presence of PtRu NPs alone or in combination with MWCNTs regarding the electroreduction of $H_2O_2$ is also obvious. The performance of *CF*–CNT/PtRu modified GC electrodes at different concentrations of $H_2O_2$ is illustrated at the FIA-grams in Fig. 7B. Based on this data and for a signal-to-noise ratio of 3, the limit of

**Table 1 – Comparative performance of GC electrodes after the modification of the electrode surface with different concentrations of PtRu NPs and *CF*–CNT/PtRu in THF. Values refer to the catalytic currents, $I_{cat}$, for the electroreduction of $H_2O_2$, corrected for the background signal ($I_b$, in the absence of $H_2O_2$), at 0.0 V in the presence of 20 mM $H_2O_2$ in 0.2 M phosphate buffer in 1 M KCl, pH 7.**

| Concentration of catalyst/mg $mL^{-1}$ | Catalyst | |
|---|---|---|
| | PtRu NPs $(I_{cat}–I_b) \times 10^{-4}$ A | *CF*–CNT/PtRu $(I_{cat}–I_b) \times 10^{-4}$ A |
| 0.0625 | 2.7 | 3.0 |
| 0.125 | 3.0 | 3.2 |
| 0.250 | 3.1 | 3.6 |
| 0.5 | 3.9 | 5.5 |
| 1 | 2.4 | 4.2 |
| 2 | 2.5 | 2.8 |

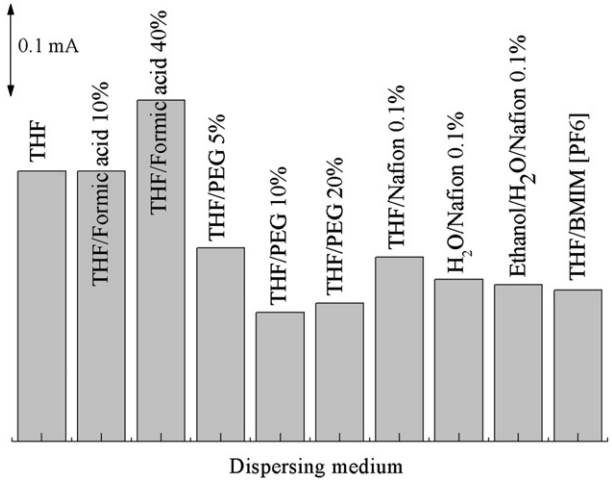


**Fig. 5 – Comparative performance of GC electrodes after the modification of the electrode surface with 1 mg/mL *CF*–CNT/PtRu in different dispersing media. Bars represent the height of the electrocatalytic currents obtained at 0.0 V in the presence of 20 mM $H_2O_2$ in 0.2 M phosphate buffer in 1 M KCl, pH 7. BMIM[$PF_6$], 1-butyl-3-methylimidazolium hexafluoroborate ionic liquid; PEG, polyethylene glycol.**

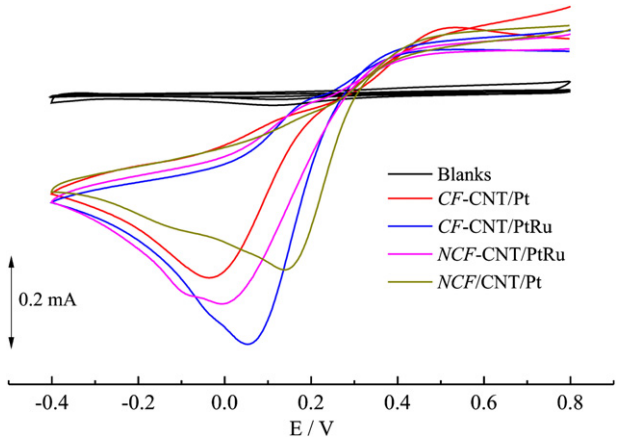


**Fig. 6 – Comparative CV-grams of the proposed GC electrodes in the absence (blank) and in the presence of 20 mM $H_2O_2$ in 0.2 M phosphate buffer in 1 M KCl, pH 7. Scan rate 100 mV/s.**

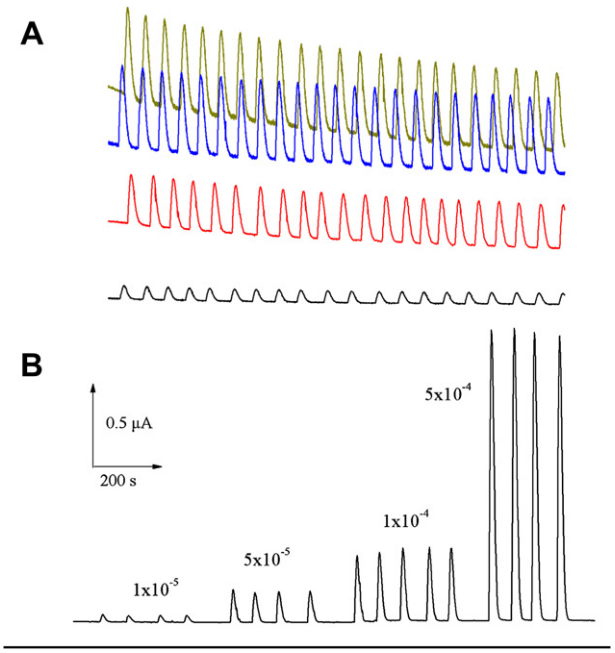


**Fig. 7 – FIA-grams of (A) 1 × $10^{-4}$ M $H_2O_2$ in 0.2 M phosphate buffer in 1 M KCl, pH 7 using a *CF*–CNT/PtRu-modified (olive line, 1–23 scans; blue line, 24–46 scans), PtRu NPs–modified (red) and bare (black) GC electrode. (B) Response of the *CF*–CNT/PtRu-modified GC electrode at different concentrations of $H_2O_2$. Applied potential 0.1 V. (For interpretation of the references to colour in this figure legend, the reader is referred to the web version of this article.)**

detection of the method was found to be 8 μM $H_2O_2$, which is adequate for most of the biosensors based applications.

### 3.2.2. *Electrocatalytic oxidation of ammonia*

The ability of the proposed hybrid materials to catalyze the electrooxidation of ammonia in strong alkaline solution (0.2 M NaOH) was also investigated with cyclic voltammetric studies. According to the comparative CV-grams, which are illustrated in Fig. 8, and taking as criterion the height of the peak current observed for each hybrid material, the tested catalysts can be classified as: *NCF*–CNT/Pt > *NCF*–CNT/PtRu > *CF*–CNT/Pt > *CF*–CNT/PtRu. In all the cases, the starting potential of the electrooxidation of $NH_3$ was observed at near −0.38 V, while in both *CF*– and *NCF*–catalysts the presence of Ru caused a decrease of the observed electrocatalytic signal, in accordance to previous studies [49]. An interesting finding of this comparative study, which deserves further investigation, is the superior behavior of the *NCF*–catalysts over the acid-treated ones.

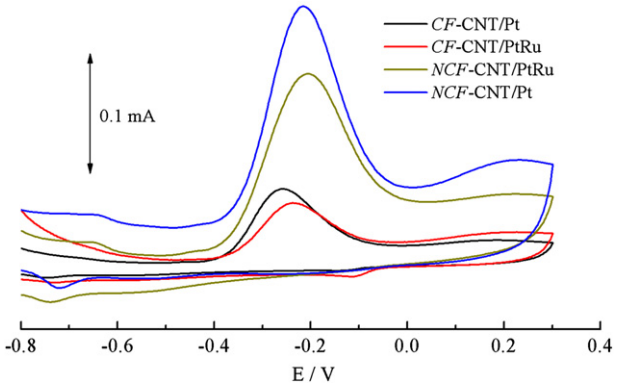


**Fig. 8 – Comparative CV-grams of ammonia oxidation on the tested hybrid materials modified GC electrodes. Test solution 0.5 M $NH_3$ in 0.2 M NaOH. Scan rate 20 mV/s.**

### 3.2.3. *Electrocatalytic oxidation of methanol*

The ability of the proposed hybrid materials to catalyze the electrooxidation of methanol in strong acidic solution (0.5 M $H_2SO_4$) was also investigated with cyclic voltammetric studies. A common observation in all the CV studies was the progressive increase of the anodic current along with a shift of the peak potential during the first 20–30 cycles. Beyond a certain scan number, which was different for each material and, sometimes, among different electrodes of the same material, a number of steady scans were recorded (about 10–20 scans), and then a progressive decrease of the anodic current was observed, suggesting that the catalysts become more poisoned as the electrode is cycled. Each CV-gram (Fig. 9) exhibited two peaks, one during the forward scan (to positive potential values), attributable to the oxidation of methanol, and one peak during the reverse scan (to negative potential values), associated with the removal of carbonaceous species not completely oxidized in the forward scan [70–72]. The ratio of the forward anodic peak current ($I_f$) to the reverse anodic

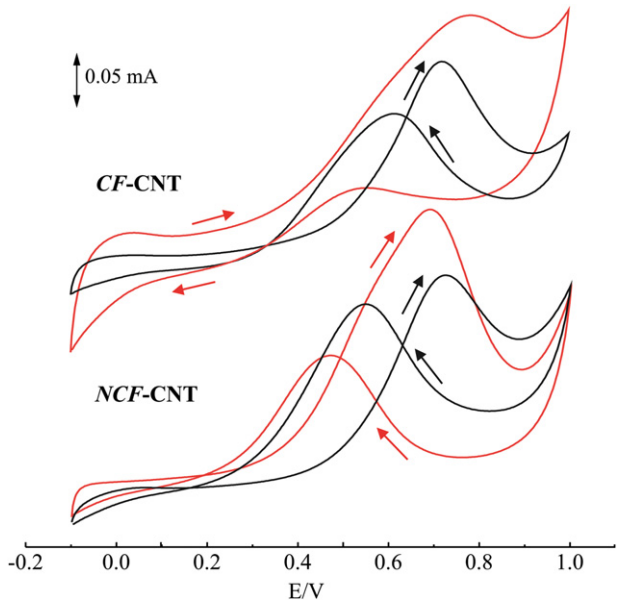


**Fig. 9 – Comparative CV-grams of methanol oxidation on the tested hybrid materials modified GC electrodes. Black line, Pt–modified catalysts; Red line PtRu–modified catalysts. Test solution 1 M $CH_3OH$ in 0.5 M $H_2SO_4$. Scan rate 20 mV/s. (For interpretation of the references to colour in this figure legend, the reader is referred to the web version of this article.)**

**Table 2 – The ratio of the forward anodic peak current ($I_f$) to the reverse anodic peak current ($I_b$), $I_f/I_b$, as it is calculated from CV-grams in Fig. 9.**

| Hybrid material | $I_f/I_b$ |
|---|---|
| *CF*–CNT/Pt | 1.3 |
| *CF*–CNT/PtRu | 2.3 |
| *NCF*–CNT/Pt | 0.9 |
| *NCF*–CNT/PtRu | 1.8 |

peak current ($I_b$), $I_f/I_b$, can be used to describe the catalyst tolerance to carbonaceous species accumulation. A higher ratio indicates more effective removal of the poisoning species on the electrode surface [70,72]. This was indeed the case for both *CF*– and *NCF*–based hybrid materials modified with the bimetallic PtRu NPs. According to previous studies [49,73,74] ruthenium dissociates water and the so produced adsorbed OH species react with adsorbed CO (poisoning species) to generate $CO_2$ (the final product of the electrooxidation of methanol). According to other studies, the electronic properties of platinum are modified by Pt–Ru orbital overlaps so that the binding strength of CO adsorbed on Pt is weakened, thus improving the overall electrocatalytic activity for the oxidation of methanol [75]. Finally, based on the $I_f/I_b$ index (Table 2), *CF*–CNT/PtRu catalyst is more efficient than *NCF*–CNT/PtRu. These findings are in agreement with Hernández-Fernández et al. [40] who demonstrated that in MWCNT-supported PtRu catalysts, the oxygen-containing groups play a beneficial role on the overall electrooxidation of methanol.

## 4. Conclusions

Functionalized MWCNTs were used as nanotemplates for the dispersion and stabilization of Pt and PtRu nanoparticles. Preformed monodispersed capped Pt and PtRu nanoparticles were attached to either covalently or non-covalently functionalized MWCNTs. The functionalization strategy showed to influence not only the chemical nature/morphology of the surfaces of nanotubes but also the electrocatalytic properties of the resulting hybrid materials. TEM images revealed the homogeneous dispersion of uniform sized NPs along the two types of functionalized MWCNT with relatively high particle density and without the formation of any noticeable aggregates while, in conjunction XRD measurements, were used to estimate the crystal structure and the mean size of the attached Pt and PtRu nanoparticles. Moreover, TEM and Raman measurements confirmed that the nanotubes remain relatively intact after chemical functionalization without showing any significant damage to their tubular graphitic structure.

The proposed hybrid materials form relatively stable suspensions in THF from which, using a simple solvent evaporation procedure, GC electrodes were properly modified to act as active surfaces for the electrochemical reduction of hydrogen peroxide and the electrochemical oxidation of ammonia and methanol. Regarding the electrochemical reduction of hydrogen peroxide the tested catalysts can be classified as: *CF*–CNT/PtRu > *NCF*–CNT/PtRu > *CF*–CNT/Pt > *NCF*–CNT/Pt. The heterogeneous catalysts containing the bimetallic catalyst PtRu were found to be the most effective, while the CNT supported catalysts perform an almost 50% higher catalytic activity compared with that observed for unsupported NPs. Concerning the electrochemical oxidation of ammonia the tested catalysts can be classified as: *NCF*–CNT/Pt > *NCF*–CNT/PtRu > *CF*–CNT/Pt > *CF*–CNT/PtRu, while *NCF*–catalysts exhibited a superior behavior over the acid-treated ones. Finally, the electrochemical oxidation of methanol both *CF*– and *NCF*–based hybrid materials modified with the bimetallic PtRu NPs found to be more effective in the removal of intermediate poising species, while based on the $I_f/I_b$ index, *CF*–CNT/PtRu catalyst turned out more efficient than *NCF*–CNT/PtRu.

## Acknowledgments

This work was partly supported by the General Secretariat of Research and Technology of Greece through the 2003 PENED program (03ED 548). The authors would like to acknowledge the use of XRD and SEM units of the Network of Laboratory Units and Centers of the University of Ioannina.

## REFERENCES

[1] Wildgoose GG, Banks CE, Compton RG. Metal nanoparticles and related materials supported on carbon nanotubes: methods and applications. Small 2006;2(2):182–93.
[2] Rao CNR, Kulkarni GU, Thomas PJ, Peter PE. Size-Dependent chemistry: properties of Nanocrystals. Chem-Eur J 2002;8(1):28–35.
[3] Hodes G. When small is different: some recent advances in concepts and applications of nanoscale phenomena. Adv Mater 2007;19(5):639–55.
[4] Gupta AK, Gupta M. Synthesis and surface engineering of iron oxide nanoparticles for biomedical applications. Biomater 2005;26(18):3995–4021.
[5] Hong H, Zhang Y, Sun J, Cai W. Molecular imaging and therapy of cancer with radiolabeled nanoparticles. Nano Today 2009;4(5):399–413.
[6] Liu S-J, Huang C-H, Huang C-K, Hwang W-S. Chelating agent-assisted heat treatment of a carbon-supported iron oxide nanoparticle catalyst for PEMFC. Chem Commun 2009;32:4809–11.
[7] Sun Y, Xia Y. Shape-Controlled synthesis of gold and silver nanoparticles. Science 2002;298(5601):2176–9.
[8] Murphy CJ, Sau TK, Gole AM, Orendorff CJ, Gao J, Gou L, et al. Anisotropic metal nanoparticles: synthesis, assembly, and Optical applications. J Phys Chem B 2005;109(29):13857–70.
[9] Xia Y, Yang P, Sun Y, Wu Y, Mayers B, Gates B, et al. One-Dimensional Nanostructures: synthesis, characterization, and applications. Adv Mater 2003;15(5):353–89.
[10] Fang XS, Ye CH, Zhang LD, Wang YH, Wu YC. Temperature-Controlled catalytic Growth of ZnS Nanostructures by the evaporation of ZnS Nanopowders. Adv Funct Mater 2005;15(1):63–8.
[11] Sun S, Zeng H. Size-Controlled synthesis of magnetite nanoparticles. J Am Chem Soc 2002;124(28):8204–5.
[12] Georgakilas V, Gournis D, Tzitzios V, Pasquato L, Guldi DM, Prato M. Decorating carbon nanotubes with metal or

semiconductor nanoparticles. J Mater Chem 2007;17(26):2679–94.
[13] Tsoufis T, Tomou A, Gournis D, Douvalis AP, Panagiotopoulos I, Kooi B, et al. Novel Nanohybrids Derived from the attachment of FePt nanoparticles on carbon nanotubes. J Nanosci Nanotechnol 2008;8(11):5942–51.
[14] Georgakilas V, Tzitzios V, Gournis D, Petridis D. Attachment of magnetic nanoparticles on carbon nanotubes and their soluble derivatives. Chem Mater 2005;17(7):1613–7.
[15] Correa-Duarte MA, Grzelczak M, Salgueirino-Maceira V, Giersig M, Liz-Marzan LM, Farle M, et al. Alignment of carbon nanotubes under low magnetic fields through attachment of magnetic nanoparticles. J Phys Chem B 2005;109(41):19060–3.
[16] Gao C, Li W, Morimoto H, Nagaoka Y, Maekawa T. Magnetic carbon Nanotubes:â€‰ synthesis by electrostatic Self-assembly approach and application in Biomanipulations. J Phys Chem B 2006;110(14):7213–20.
[17] Jia B, Gao L, Sun J. Self-assembly of magnetite beads along multiwalled carbon nanotubes via a simple hydrothermal process. Carbon 2007;45(7):1476–81.
[18] Wang H, Cao L, Yan S, Huang N, Xiao Z. An efficient method for decoration of the multiwalled carbon nanotubes with nearly monodispersed magnetite nanoparticles. Mater Sci Eng B 2009;164(3):191–4.
[19] Ahn H-J, Moon WJ, Seong T-Y, Wang D. Three-dimensional nanostructured carbon nanotube array/PtRu nanoparticle electrodes for micro-fuel cells. Electrochem Commun 2009;11(3):635–8.
[20] Scott K, Shukla AK. Modern Aspects of Electrochemistry, vol. 40. Berlin: Springer; 2007.
[21] Aricò AS, Srinivasan S, Antonucci V. DMFCs: from fundamental Aspects to technology development. Fuel Cells 2001;1(2):133–61.
[22] Chetty R, Xia W, Kundu S, Bron M, Reinecke T, Schuhmann W, et al. Effect of reduction temperature on the preparation and characterization of Pt-Ru nanoparticles on multiwalled carbon nanotubes. Langmuir 2009;25(6):3853–60.
[23] Huang J-E, Guo D-J, Yao Y-G, Li H-L. High dispersion and electrocatalytic properties of platinum nanoparticles on surface-oxidized single-walled carbon nanotubes. J Electroanal Chem 2005;577(1):93–7.
[24] Maxakato NW, Arendse CJ, Ozoemena KI. Insights into the electro-oxidation of ethylene glycol at Pt/Ru nanocatalysts supported on MWCNTs: adsorption-controlled electrode kinetics. Electrochem Commun 2009;11(3):534–7.
[25] Maxakato NW, Ozoemena KI, Arendse CJ. Dynamics of electrocatalytic oxidation of ethylene glycol, methanol and formic acid at MWCNT platform electrochemically modified with Pt/Ru nanoparticles. Electroanalysis 2010;22(5):519–29.
[26] Yi-Fan H, Yu-Chi H, Pu-Wei W, Chen-Hong L, Yun-Min C. Pulse Electrodepositions of PtRu on Large-area carbon nanotubes for enhancement of methanol electro-oxidation. J Electrochem Soc 2010;157(1):B39–44.
[27] Hsu Y-K, Yang J-L, Lin Y-G, Chen S-Y, Chen L-C, Chen K-H. Electrophoretic deposition of PtRu nanoparticles on carbon nanotubes for methanol oxidation. Diamond Relat Mater 2009;18(2–3):557–62.
[28] Xiao F, Zhao F, Mei D, Mo Z, Zeng B. Nonenzymatic glucose sensor based on ultrasonic-electrodeposition of bimetallic PtM (M = Ru, Pd and Au) nanoparticles on carbon nanotubes-ionic liquid composite film. Biosens Bioelectron 2009;24(12):3481–6.
[29] Choi HC, Shim M, Bangsaruntip S, Dai H. Spontaneous reduction of metal Ions on the Sidewalls of carbon nanotubes. J Am Chem Soc 2002;124(31):9058–9.
[30] Hsieh CT, Lin JY, Wei JL. Deposition and electrochemical activity of Pt-based bimetallic nanocatalysts on carbon nanotube electrodes. Int J Hydrogen Energy 2009;34(2):685–93.
[31] Jiang S, Zhu L, Ma Y, Wang X, Liu J, Zhu J, et al. Direct immobilization of Pt-Ru alloy nanoparticles on nitrogen-doped carbon nanotubes with superior electrocatalytic performance. J Power Sources 2011;195(22):7578–82.
[32] Guo D-J. Novel synthesis of PtRu/multi-walled carbon nanotube catalyst via a microwave-assisted imidazolium ionic liquid method for methanol oxidation. J Power Sources 2010;195(21):7234–7.
[33] Liu Z, Ling XY, Guo B, Hong L, Lee JY. Pt and PtRu nanoparticles deposited on single-wall carbon nanotubes for methanol electro-oxidation. J Power Sources 2007;167(2):272–80.
[34] Esmaeilifar A, Yazdanpour M, Rowshanzamir S, Eikani MH. Hydrothermal synthesis of Pt/MWCNTs nanocomposite electrocatalysts for proton exchange membrane fuel cell systems. Int J Hydrogen Energy 2011;36(9):5500–11.
[35] Liu Z, Lee JY, Chen W, Han M, Gan LM. Physical and electrochemical Characterizations of microwave-assisted polyol preparation of carbon-supported PtRu nanoparticles. Langmuir 2003;20(1):181–7.
[36] Hsu N-Y, Chien C-C, Jeng K-T. Characterization and enhancement of carbon nanotube-supported PtRu electrocatalyst for direct methanol fuel cell applications. Appl Catal B 2008;84(1–2):196–203.
[37] Xu M-W, Su Z, Weng Z-W, Wang Z-C, Dong B. An approach for synthesizing PtRu/MWCNT nanocomposite for methanol electro-oxidation. Mater Chem Phys 2010;124(1):785–90.
[38] Zhou Z, Li W, Guo P, Yang H, Xiang X, Zeng L, et al. Catalytic activity and stability toward methanol oxidation of PtRu/CNTs prepared by adsorption in aqueous solution and reduction in ethylene glycol. J Solid State Electrochem 2010;14(2):191–6.
[39] Hrapovic S, Liu Y, Male KB, Luong JHT. Electrochemical biosensing Platforms using platinum nanoparticles and carbon nanotubes. Anal Chem 2003;76(4):1083–8.
[40] Hernandez-Fernandez P, Nuono R, Fatas E, Fierro JLG, Ocon P. MWCNT-supported PtRu catalysts for the electrooxidation of methanol: effect of the functionalized support. Int J Hydrogen Energy 2011;36(14):8267–78.
[41] Ahmadi R, Amini MK. Synthesis and characterization of Pt nanoparticles on sulfur-modified carbon nanotubes for methanol oxidation. Int J Hydrogen Energy 2011;36(12):7275–83.
[42] Park SJ, Lee SY. Hydrogen storage behaviors of platinum-supported multi-walled carbon nanotubes. Int J Hydrogen Energy 2010;35(23):13048–54.
[43] Chen Y, Zhang G, Ma J, Zhou Y, Tang Y, Lu T. Electro-oxidation of methanol at the different carbon materials supported Pt nano-particles. Int J Hydrogen Energy 2010;35(19):10109–17.
[44] Jha N, Leela Mohana Reddy A, Shaijumon MM, Rajalakshmi N, Ramaprabhu S. Pt-Ru/multi-walled carbon nanotubes as electrocatalysts for direct methanol fuel cell. Int J Hydrogen Energy 2008;33(1):427–33.
[45] Marincic L, Leitz FB. Electro-oxidation of ammonia in waste water. J Appl Electrochem 1978;8(4):333–45.
[46] Timmer BH, Van Delft KM, Otjes RP, Olthuis W, Van Den Berg A. Miniaturized measurement system for ammonia in air. Anal Chim Acta 2004;507(1):137–43.
[47] Choudhary TV, Sivadinarayana C, Goodman DW. Production of COx-free hydrogen for fuel cells via step-wise hydrocarbon reforming and catalytic dehydrogenation of ammonia. Chem Engineer J 2003;93(1):69–80.
[48] Gerischer H, Mauerer A. Untersuchungen zur anodischen oxidation von ammoniak an platin-elektroden. J Electroanal Chem 1970;25(3):421–33.

[49] Vidal-Iglesias FJ, Solla-Gullon J, Montiel V, Feliu JM, Aldaz A. Screening of electrocatalysts for direct ammonia fuel cell: ammonia oxidation on PtMe (Me: Ir, Rh, Pd, Ru) and preferentially oriented Pt(1 0 0) nanoparticles. J Power Sources 2007;171(2):448–56.
[50] De Vooys ACA, Koper MTM, Van Santen RA, Van Veen JAR. The role of adsorbates in the electrochemical oxidation of ammonia on noble and transition metal electrodes. J Electroanal Chem 2001;506(2):127–37.
[51] Endo K, Nakamura K, Katayama Y, Miura T. Pt-Me (Me = Ir, Ru, Ni) binary alloys as an ammonia oxidation anode. Electrochim Acta 2004;49(15):2503–9.
[52] Prodromidis MI, Karayannis MI. Enzyme based amperometric biosensors for food analysis. Electroanalysis 2002;14(4):241–61.
[53] Rong LQ, Yang C, Qian QY, Xia XH. Study of the nonenzymatic glucose sensor based on highly dispersed Pt nanoparticles supported on carbon nanotubes. Talanta 2007; 72(2):819–24.
[54] Zhang J, Liu P, Ma H, Ding Y. Nanostructured porous gold for methanol electro-oxidation. J Phys Chem C 2007;111(28): 10382–8.
[55] Lee YJ, Park JY, Kim Y, Ko JW. Amperometric sensing of hydrogen peroxide via highly roughened macroporous Gold-/ Platinum nanoparticles electrode. Curr Appl Phys 2011;11(2): 211–6.
[56] He X, Hu C, Liu H, Du G, Xi Y, Jiang Y. Building Ag nanoparticle 3D catalyst via Na2Ti3O7 nanowires for the detection of hydrogen peroxide. Sens Actuators B 2010; 144(1):289–94.
[57] Liu S, Ju H. Reagentless glucose biosensor based on direct electron transfer of glucose oxidase immobilized on colloidal gold modified carbon paste electrode. Biosens Bioelectron 2003;19(3):177–83.
[58] Huang J, Wang D, Hou H, You T. Electrospun palladium nanoparticle-loaded carbon nanofibers and their electrocatalytic activities towards hydrogen peroxide and NADH. Adv Funct Mater 2008;18(3):441–8.
[59] You JM, Jeong YN, Ahmed MS, Kim SK, Choi HC, Jeon S. Reductive determination of hydrogen peroxide with MWCNTs-Pd nanoparticles on a modified glassy carbon electrode. Biosens Bioelectron 2011;26(5):2287–91.
[60] Tomou A, Panagiotopoulos I, Gournis D, Kooi B. L1(0) ordering and magnetic interactions in FePt nanoparticles embedded in MgO and SiO2 shell matrices. J Appl Phys 2007; 102(2):023910.
[61] Pavlidis IV, Tsoufis T, Enotiadis A, Gournis D, Stamatis H. Functionalized multi-wall carbon nanotubes for lipase immobilization. Adv Engineer Mater 2010;12(5):B179–83.
[62] Li X, Liu Y, Fu L, Cao L, Wei D, Wang Y. Efficient synthesis of carbon Nanotube–Nanoparticle hybrids. Adv Funct Mater 2006;16(18):2431–7.
[63] Hills CW, Mack NH, Nuzzo RG. The size-dependent structural phase behaviors of supported bimetallic (Pt-Ru) nanoparticles. J Phys Chem B 2003;107(12):2626–36.
[64] Bock C, Paquet C, Couillard M, Botton GA, MacDougall BR. Size-Selected synthesis of PtRu nano-catalysts: reaction and size control mechanism. J Am Chem Soc 2004;126(25): 8028–37.
[65] Yao Y-l, Ding Y, Ye L-S, Xia X-H. Two-step pyrolysis process to synthesize highly dispersed Pt-Ru/carbon nanotube catalysts for methanol electrooxidation. Carbon 2006;44(1): 61–6.
[66] Gu Y-J, Wong W-T. Nanostructure PtRu/MWNTs as anode catalysts prepared in a vacuum for direct methanol oxidation. Langmuir 2006;22(26):11447–52.
[67] Chen SY, Miao HY, Lue JT, Ouyang MS. Fabrication and field emission property studies of multiwall carbon nanotubes. J Phys D-Appl Phys 2004;37(2):273–9.
[68] Murphy H, Papakonstantinou P, Okpalugo TIT. Raman study of multiwalled carbon nanotubes functionalized with oxygen groups. J Vac Sci Technol B 2006;24(2):715–20.
[69] Georgakilas V, Bourlinos A, Gournis D, Tsoufis T, Trapalis C, Mateo-Alonso A, et al. Multipurpose organically modified carbon nanotubes: from functionalization to nanotube composites. J Am Chem Soc 2008;130(27):8733–40.
[70] Qin YH, Yang HH, Zhang XS, Li P, Ma CA. Effect of carbon nanofibers microstructure on electrocatalytic activities of Pd electrocatalysts for ethanol oxidation in alkaline medium. Int J Hydrogen Energy 2010;35(15):7667–74.
[71] Singh RN, Singh A. Anindita. Electrocatalytic activity of binary and ternary composite films of Pd, MWCNT and Ni, Part II: methanol electrooxidation in 1 M KOH. Int J Hydrogen Energy 2009;34(4):2052–7.
[72] Zhao YC, Zhan L, Tian JN, Nie SL, Ning Z. Enhanced electrocatalytic oxidation of methanol on Pd/polypyrrole-graphene in alkaline medium. Electrochim Acta 2011;56(5): 1967–72.
[73] Holstein WL, Rosenfeld HD. In-Situ X-ray absorption spectroscopy study of Pt and Ru chemistry during methanol Electrooxidationâ€. J Phys Chem B 2004;109(6):2176–86.
[74] Jingyu S, Jianshu H, Yanxia C, Xiaogang Z. Hydrotermal synthesis of Pt-Ru/MWCNTs and its electrocatalytic properties for oxidation of methanol. Int J Electrochem Sci 2007;2:64–71.
[75] Oetjen HF, Schmidt VM, Stimming U, Trila F. Performance data of a proton exchange membrane fuel cell using $H_2$/CO as fuel gas. J Electrochem Soc 1996;143(12):3838–42.